AGU PUBLICATIONS

JGR

Journal of Geophysical Research: Solid Earth

RESEARCH ARTICLE
10.1002/2014JB011775

This article is a companion to *Neri et al.* [2015] doi:10.1002/2014JB011776.

Key Points:
- Probability of vent opening is higher in the central eastern part of the caldera
- Vent opening probability is widely spread all over the caldera
- Some sources of uncertainty were identified and quantified by expert judgment

Supporting Information:
- Text S1
- Table S1
- Table S2
- Data Set S1
- Data Set S2
- Data Set S3

Correspondence to:
A. Neri,
augusto.neri@ingv.it

Citation:
Bevilacqua, A., et al. (2015), Quantifying volcanic hazard at Campi Flegrei caldera (Italy) with uncertainty assessment: 1. Vent opening maps, *J. Geophys. Res. Solid Earth*, *120*, 2309–2329, doi:10.1002/2014JB011775.

Received 23 NOV 2014
Accepted 13 MAR 2015
Accepted article online 19 MAR 2015
Published online 22 APR 2015

Quantifying volcanic hazard at Campi Flegrei caldera (Italy) with uncertainty assessment: 1. Vent opening maps

Andrea Bevilacqua[1,2], Roberto Isaia[3], Augusto Neri[1], Stefano Vitale[4], Willy P. Aspinall[5,6], Marina Bisson[1], Franco Flandoli[7], Peter J. Baxter[8], Antonella Bertagnini[1], Tomaso Esposti Ongaro[1], Enrico Iannuzzi[3], Marco Pistolesi[9,10], and Mauro Rosi[10,11]

[1]Istituto Nazionale di Geofisica e Vulcanologia, Sezione di Pisa, Pisa, Italy, [2]Scuola Normale Superiore, Pisa, Italy, [3]Istituto Nazionale di Geofisica e Vulcanologia, Osservatorio Vesuviano, Napoli, Italy, [4]Università di Napoli "Federico II", Dipartimento di Scienze della Terra, dell'Ambiente e delle Risorse, Napoli, Italy, [5]University of Bristol, School of Earth Sciences, Bristol, UK, [6]Aspinall & Associates, Tisbury, UK, [7]Università di Pisa, Dip.to di Matematica, Pisa, Italy, [8]University of Cambridge, Institute of Public Health, Cambridge, UK, [9]Università di Firenze, Dip.to di Scienze della Terra, Firenze, Italy, [10]Università di Pisa, Dip.to di Scienze della Terra, Pisa, Italy, [11]Dipartimento della Protezione Civile, Roma, Italy

Abstract Campi Flegrei is an active volcanic area situated in the Campanian Plain (Italy) and dominated by a resurgent caldera. The great majority of past eruptions have been explosive, variable in magnitude, intensity, and in their vent locations. In this hazard assessment study we present a probabilistic analysis using a variety of volcanological data sets to map the background spatial probability of vent opening conditional on the occurrence of an event in the foreseeable future. The analysis focuses on the reconstruction of the location of past eruptive vents in the last 15 ka, including the distribution of faults and surface fractures as being representative of areas of crustal weakness. One of our key objectives was to incorporate some of the main sources of epistemic uncertainty about the volcanic system through a structured expert elicitation, thereby quantifying uncertainties for certain important model parameters and allowing outcomes from different expert weighting models to be evaluated. Results indicate that past vent locations are the most informative factors governing the probabilities of vent opening, followed by the locations of faults and then fractures. Our vent opening probability maps highlight the presence of a sizeable region in the central eastern part of the caldera where the likelihood of new vent opening per kilometer squared is about 6 times higher than the baseline value for the whole caldera. While these probability values have substantial uncertainties associated with them, our findings provide a rational basis for hazard mapping of the next eruption at Campi Flegrei caldera.

1. Introduction

Campi Flegrei (CF) is a volcanic caldera with a diameter of about 12 km and the town of Pozzuoli at its center (Figure 1) [*Rittmann*, 1950; *Rosi and Sbrana*, 1987; *Orsi et al*., 2004]. The northern and western parts of the caldera are above sea level and characterized by the presence of many dispersed cones and craters, whereas the southern part is principally submarine and extends into Golfo di Pozzuoli. CF is the most active caldera in Europe having had more than 70 eruptions within the last 15 ka [*Rosi et al*., 1983; *Di Vito et al*., 1999; *Orsi et al*., 2004; *Isaia et al*., 2009; *Smith et al*., 2011]. Activity started more than 80 ka B.P. [*Scarpati et al*., 2012; *Vitale and Isaia*, 2014] and includes the generation of the large caldera-collapse Campanian Ignimbrite eruption (CI, ~40 ka B.P.) [*De Vivo et al*., 2001; *Giaccio et al*., 2008] and the second major caldera-collapse eruption of the Neapolitan Yellow Tuff (NYT, ~15 ka B.P.) [*Orsi et al*., 1992; *Deino et al*., 2004]. In the last 15 ka, intense and mostly explosive volcanism and deformation has occurred within the NYT caldera, along its structural boundaries as well as along faults within the caldera (Figure 2) [*Di Vito et al*., 1999; *Orsi et al*., 2004; *Isaia et al*., 2009; *Smith et al*., 2011]. Eruptions were closely spaced in time, over periods from a few centuries to a few millennia, with periods of quiescence lasting several millennia. As a consequence, activity has been generally subdivided into three distinct epochs, i.e., Epoch I, 15–10.6 ka; Epoch II, 9.6–9.1 ka; and Epoch III, 5.5–3.8 ka B.P. [*Orsi et al*., 2004; *Smith et al*., 2011]. Simultaneous eruptions from different sectors of the caldera have also occurred at least during the Epoch III [*Isaia et al*., 2009]. The most recent eruption was that of Monte Nuovo in 1538 A.D. [*Di Vito et al*., 1987; *D'Oriano et al*., 2005; *Guidoboni and Ciuccarelli*, 2011]. Volcanism was also

Figure 1. Mosaic of orthophotos of Campi Flegrei caldera and surrounding areas (including the city of Naples on the east) showing the large urbanization inside and around this active volcano [*Bisson et al*., 2007].

generally preceded by broadly distributed ground deformation phenomena leading to remarkable uplift of the central part of the caldera (e.g., larger than 100 m in the last 10.5 ka [*Di Vito et al*., 1999; *Isaia et al*., 2009] and several meters before the Monte Nuovo eruption [*Dvorak and Gasparini*, 1991; *Guidoboni and Ciuccarelli*, 2011]).

In recent decades, CF has exhibited significant deformation phenomena in the central part of the caldera that produced a dome-like structure having a base diameter of about 6–7 km with an uplift of several tens of meters from the sea bottom, centered on the town of Pozzuoli [*Berrino et al*., 1984; *Del Gaudio et al*., 2010]. For instance, in 1982–1984, there was rapid uplift of the center of the caldera of about 1.8 m. Since then, the caldera surface has been slowly subsiding, but punctuated by significant uplift episodes. Changes in the gas composition of fumaroles were measured in 2006 and again in 2011–2012 [*Chiodini et al*., 2012]. Based on the above information, and with more than 300,000 people living within the caldera, the volcanic risk at CF is considered to be substantial.

Defining likely locations of future vents is a key scientific goal for hazard and risk assessment, especially given the wide dispersion of past eruptive vents within the caldera. *Alberico et al*. [2002] presented a first quantitative analysis, based on seven geophysical, geological, and geochemical parameters, each one assumed to be representative of a degree of anomaly. These parameters were combined to produce a spatial distribution of the probability of vent opening on a regular grid with cells of side 1 km, covering the whole caldera. Their findings suggested that the inner portion of the caldera (approximately a circular area with a diameter of about 6 km centered on the town of Pozzuoli) had the highest probability of vent opening. In contrast, *Orsi et al*. [2004] assumed, mostly on structural considerations, that the chances of a new vent opening depended only on the distribution of past vents of Epoch III. They qualitatively identified two distinct areas, one with higher probability of vent opening (approximately located in the region of Astroni, Agnano, and part of San Vito) and the other with lower probability (approximately located in the area of Averno and Monte Nuovo). More recently, *Selva et al*. [2012] produced a probabilistic map, over a regular grid with cells of sides 500 m, based on a Bayesian inference procedure and reporting uncertainty ranges for probability values. Their approach included information on the location of past vents of Epoch III, starting from a prior distribution defined by assigning scores to the presence of tectonic structures or eruptive vents of the last 15 ka in the NYT caldera. This

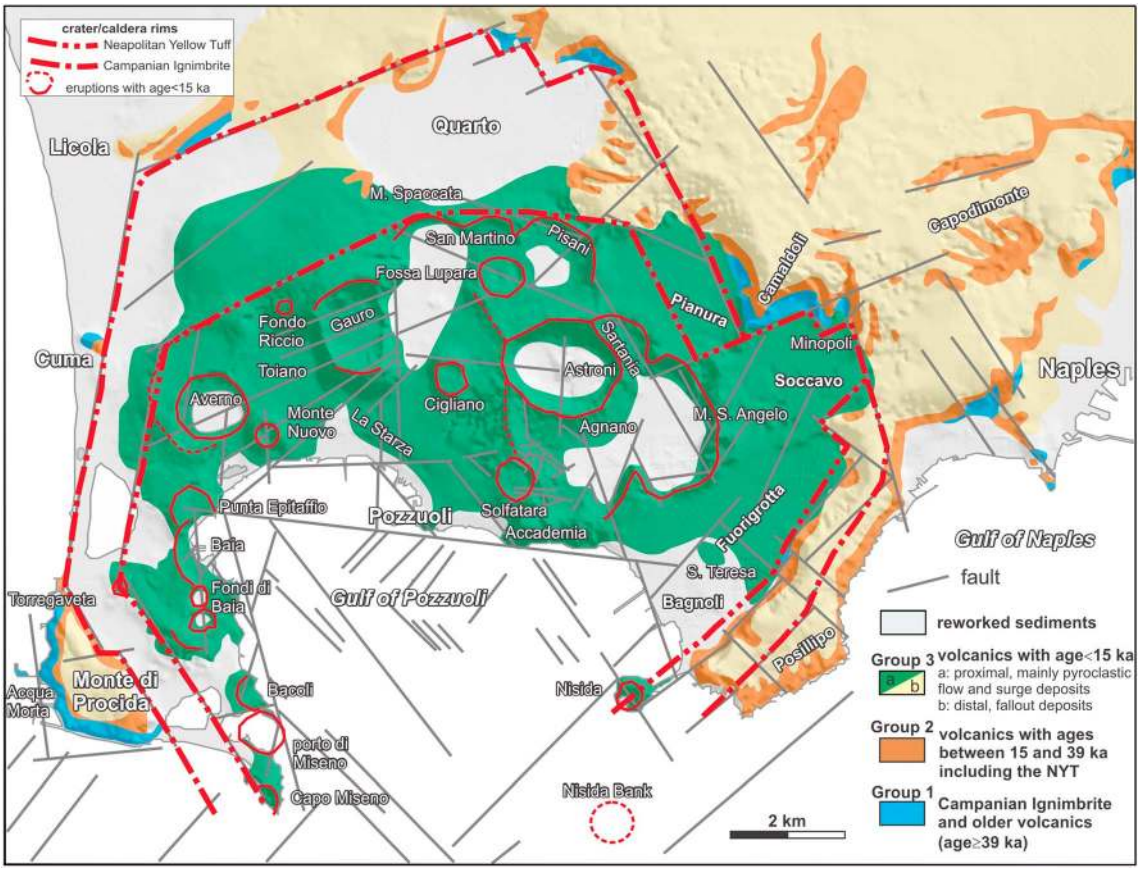

Figure 2. Simplified geological map of Campi Flegrei caldera showing regional fault traces and main morphological structures such as caldera and crater rims and faults derived from sea seismic profiles [from *Vitale and Isaia* 2014].

study highlighted how the probability of vent opening is widely distributed over the caldera, with two areas of higher probability of vent opening located in the Agnano-Astroni-San Vito and the Averno-Monte Nuovo areas.

The goal of the present study is to produce a new background (sometimes also referred to as long-term or base rate) probability map of vent opening of the caldera by incorporating information from some of the most recent studies of CF, specifically focusing on some of the key epistemic uncertainties of the volcanic system. In particular, the produced maps express the probability of vent opening conditional on the occurrence of a new eruption in the foreseeable future. This is done by considering the eruptive record of CF in the last 15 ka as well as the distribution of key structural features, such as faults and fractures, within the caldera. The probability model that we assumed is doubly stochastic, in the sense that the probability values representing the spatial aleatoric variability (or uncertainty) affecting the vent opening process are themselves affected by epistemic uncertainty. The sources of epistemic uncertainty considered relate to the uncertain locations of past vents, the incompleteness of the eruptive record, and uncertain weights given to the different volcanic system variables under consideration. We based the uncertainty quantification on a structured elicitation with alternative pooling procedures, thus creating percentile maps associated with the sources of epistemic uncertainty considered in addition to a map of mean probability. This approach is of critical importance since it provides, together with the collected monitoring data, the framework for mapping short-term vent openings and, most importantly, is the starting point for making probabilistic hazard maps for the main hazardous phenomena that could be related to this caldera, such as pyroclastic density currents (PDCs) and ash fallout. In the companion paper [*Neri et al.*, 2015] we describe its application to show the underlying probabilities of future vent locations in hazard maps of PDC invasion potential together with estimates of their uncertainty.

2. Method

We followed a structured expert elicitation and judgment pooling approach [e.g., *Cooke*, 1991; *Aspinall*, 2006] to quantify epistemic uncertainties on evidence coming from different strands of volcanological data and then merge these distributions to produce a doubly stochastic probabilistic vent opening map that accommodates and expresses these different sources of uncertainty. Our method is based on the assumption that the probability of new vent opening can be computed as a weighted linear combination of the spatial distributions of key physical variables of the system that reflect, or can influence, this volcanic process. Similar approaches, but involving different techniques, have been applied by *Selva et al*. [2012] and by *Bartolini et al*. [2013] for mapping vent opening at explosive volcanoes and by *Martì and Felpeto* [2010], *Cappello et al*. [2012], and *Connor et al*. [2012] for generating vent opening maps (also called susceptibility maps, e.g., *Martì and Felpeto* [2010]) at effusive volcanoes. A similar approach has also applied for the generation of ensemble maps of seismic and tectonic hazards for planning geological areas suited for radioactive waste storage or disposal [e.g., *Chapman et al*., 2012].

We used data from literature and new data reported here. The variables considered in the analysis were the distribution of the eruptive vents opened during the three epochs in the last 15 ka of activity of the volcano, the distribution of maximum fault dislocations, and the density of surface fractures over the whole caldera. Based on the present understanding of caldera systems, these five distributions, representative of the aleatoric variability of the vent opening process, appear to be the ones most closely correlated with vent opening potential, with faults and fractures representative of near-surface regions of crustal weakness in the caldera. We acknowledge that the probability of new intracaldera vent opening could be correlated with other system variables or processes that we did not consider due to lack of knowledge about them. To account for any contribution from these neglected factors and to represent missing information, we included a conservative spatial uniform distribution inside the NYT caldera. The analysis focused on events from the last 15 ka of activity of the volcano since these are by far the best known and, given the volcanological and structural evolution of the caldera [*Rosi et al*., 1983; *Di Vito et al*., 1999; *Orsi et al*., 2004], are also the most relevant for this study. In fact we presumed that the caldera did not evolved significantly over this interval; moreover, some differential weighting, from the elicitation findings, was applied which tested the effect of placing more emphasis on the most recent data.

A key aspect of the study was the identification, and where possible the quantification, of some of the main sources of epistemic uncertainty that are associated with the available data and therefore need to be reflected in the final maps. In particular, in reconstruction from deposits the attendant uncertainty on location of related eruptive vents was considered, as were the number of past events which do not correspond to presently identified vents but which do exist in the stratigraphic evidences (so-called *lost vents*) and the uncertainty of linear weights to be associated with the variables that contribute to the definition of the mapping. With regards to the uncertainty of the weights and unknown values of some other variables, we adopted a simple logic tree of questions and different scoring rule models for pooling group judgments, including performance-based (Appendix A) [e.g., *Cooke*, 1991; *Aspinall*, 2006; *Flandoli et al*., 2011; *Chapman et al*., 2012] and equal weight models. The procedure differs from previous studies where the weights were deterministically assigned by the authors to variables with unknown values [e.g., *Selva et al*., 2012; *Bartolini et al*., 2013].

3. The Volcanological Data Sets

Inputs to the probabilistic maps consist of three different types of data sets: (1) the spatial distribution of vent opening locations in the three epochs of the last 15 ka, (2) the spatial distribution of maximum fault displacement, and (3) the surface fracture density. Unless reported otherwise, all three variables were mapped on a regular grid of 100×100 cells of side 250 m, covering the whole caldera, with the lower left corner of the grid at (415,000, 4,510,000) WGS84 universal time meridian Zone 33 coordinates. As the outer boundary of the analysis we considered the rim of the CI caldera as reconstructed by *Vitale and Isaia* [2014] since all vents of the last 15 ka were inside it and even faults and fractures outside this area appear old and not correlated with the most recent volcanic activity.

3.1. Distributions of Past Vents

The location of past vents represents the principal information to consider when constructing a vent opening probability map. Therefore, this variable was investigated in depth trying to quantify the different sources of

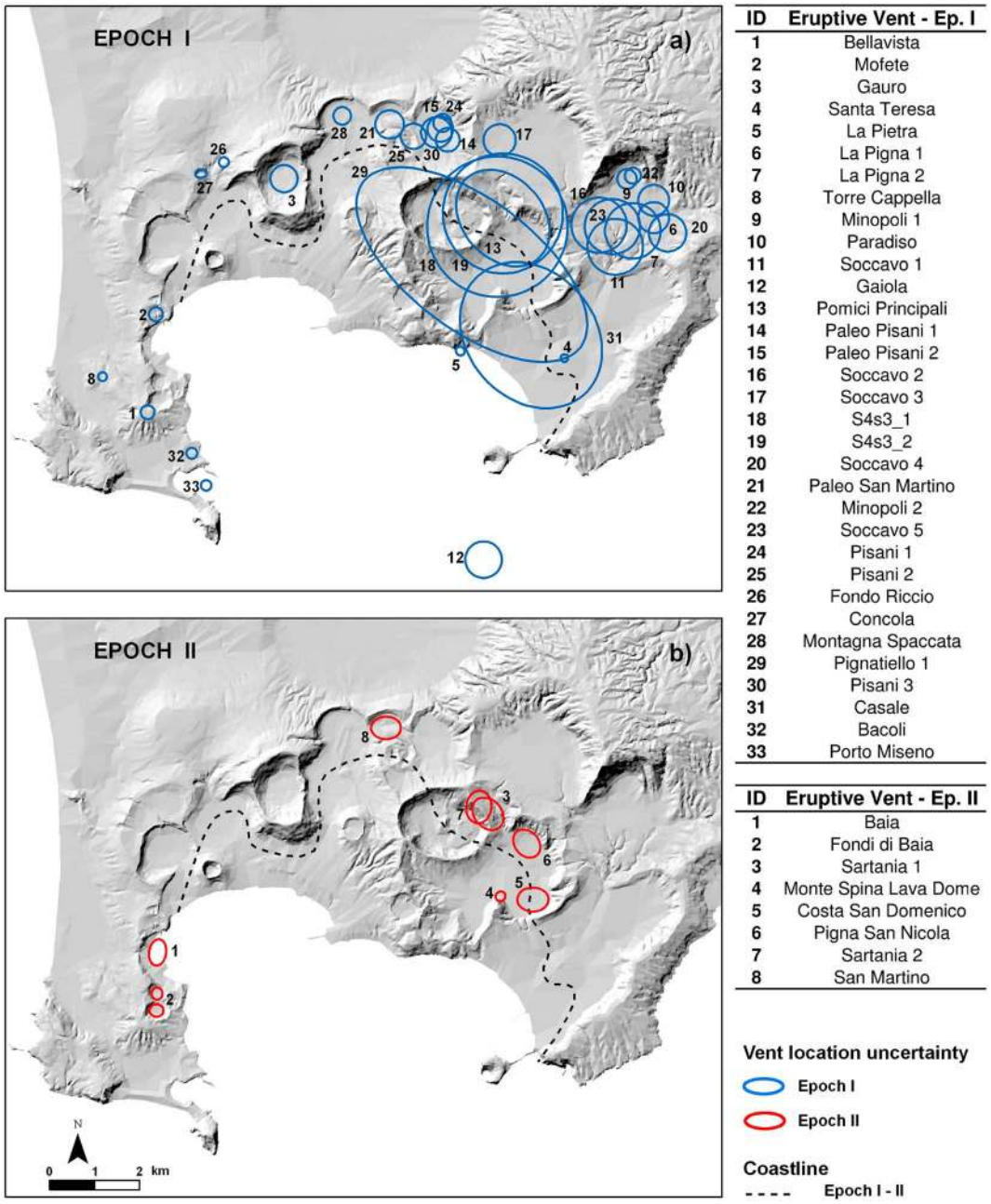

ID	Eruptive Vent - Ep. I
1	Bellavista
2	Mofete
3	Gauro
4	Santa Teresa
5	La Pietra
6	La Pigna 1
7	La Pigna 2
8	Torre Cappella
9	Minopoli 1
10	Paradiso
11	Soccavo 1
12	Gaiola
13	Pomici Principali
14	Paleo Pisani 1
15	Paleo Pisani 2
16	Soccavo 2
17	Soccavo 3
18	S4s3_1
19	S4s3_2
20	Soccavo 4
21	Paleo San Martino
22	Minopoli 2
23	Soccavo 5
24	Pisani 1
25	Pisani 2
26	Fondo Riccio
27	Concola
28	Montagna Spaccata
29	Pignatiello 1
30	Pisani 3
31	Casale
32	Bacoli
33	Porto Miseno

ID	Eruptive Vent - Ep. II
1	Baia
2	Fondi di Baia
3	Sartania 1
4	Monte Spina Lava Dome
5	Costa San Domenico
6	Pigna San Nicola
7	Sartania 2
8	San Martino

Figure 3. Reconstruction of the location of the eruptive vents and fissures for the events occurred in (a) Epoch I and (b) Epoch II. Numbered circles and ellipses indicate the assumed vent location of the events listed on the right side of the maps. The name of the events follows *Smith et al.* [2011]. The dashed line indicates the likely location of the coast line between Epochs II and III [from *Orsi et al.*, 2004].

uncertainty that affect it. In particular, we focused on the uncertain location of the vents which, in most cases, cannot be represented as precise points, and on the uncertain number of vents that might have existed but now are not visible (lost vents).

The locations of vents for the eruptive events that occurred in Epochs I, II, and III (Figures 3 and 4) are indicated on the maps by circles or ellipses representing the area where the eruptive vent (or fissure) was probably located during the eruption. Small circles/ellipses indicate a good knowledge of the vent location, mostly based on the existence of a crater, the presence of other surface morphological features, or a well-exposed areal

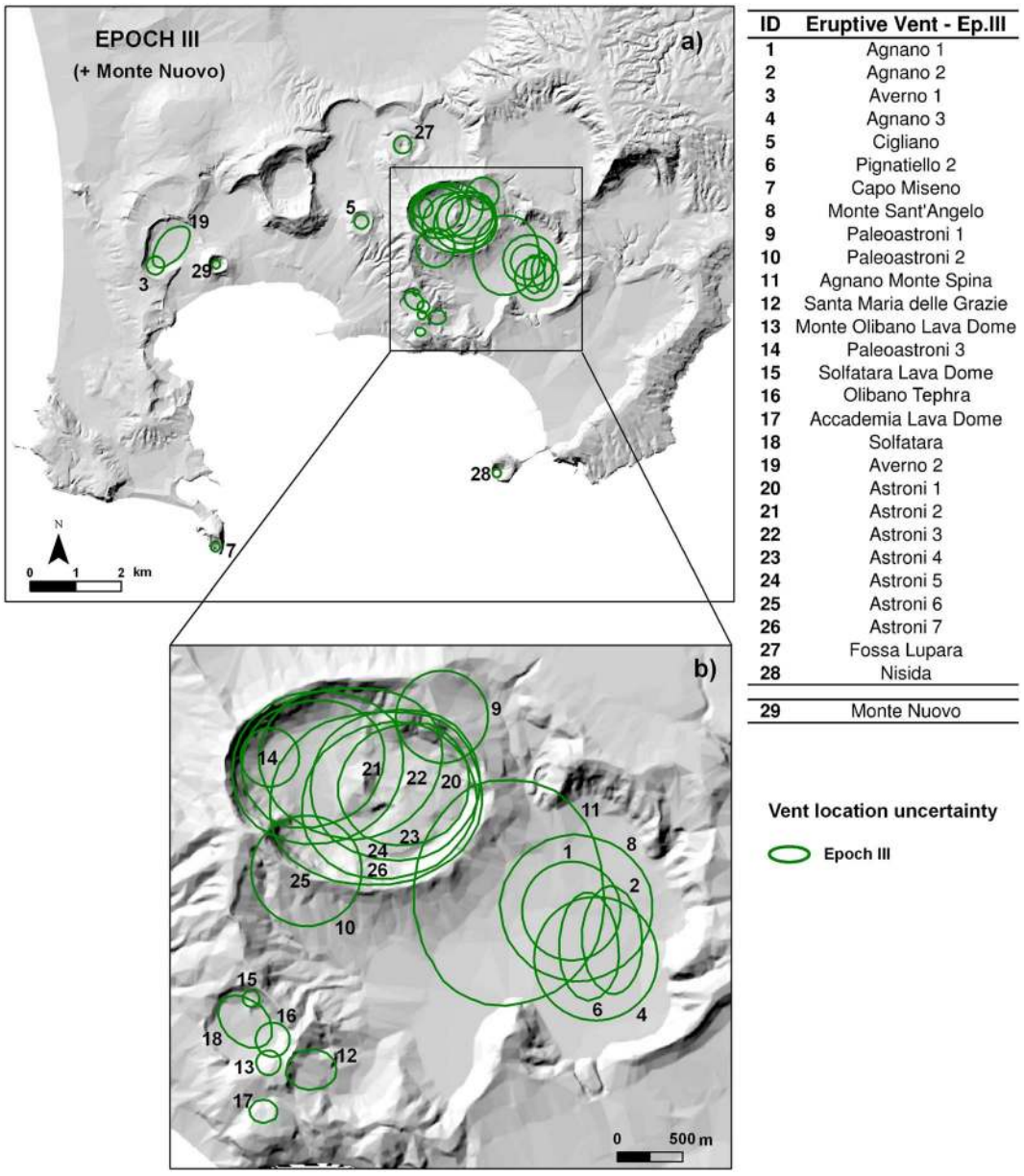

Figure 4. (a) Reconstruction of the location of the eruptive vents and fissures for the events occurred in Epoch III and of the Monte Nuovo eruption. (b) The map represents an enlargement of the area of Agnano-Astroni-Solfatara where many events occurred. Numbered circles and ellipses indicate the assumed vent location of the events listed on the right side of the maps. The name of the events follows *Smith et al.* [2011].

deposit distribution. Large circles/ellipses indicate large uncertainty in vent location due to burial or destruction by subsequent eruptions, or by the action of seawater inundating the caldera. Migration of a vent during the same eruptive event was also considered and, where this was considered plausible, contributed to a large vent location ellipse. We defined the vent location data set by assuming a one-to-one relationship between the eruptive event (assumed as deposit erupted in a period of time representative of the eruption duration, i.e., of the order of days/months) and the eruptive vent from which it originated. The possible occurrence of eruptions with two simultaneously active vents in different sectors of the caldera was considered as two distinct events for the aim of vent zonation (see *Neri et al.* [2015] for further considerations about this possibility). During Epoch I the recognized vents were mostly concentrated along the northern and eastern border portions of the caldera (Figure 3), whereas during Epochs II and III volcanism was mostly

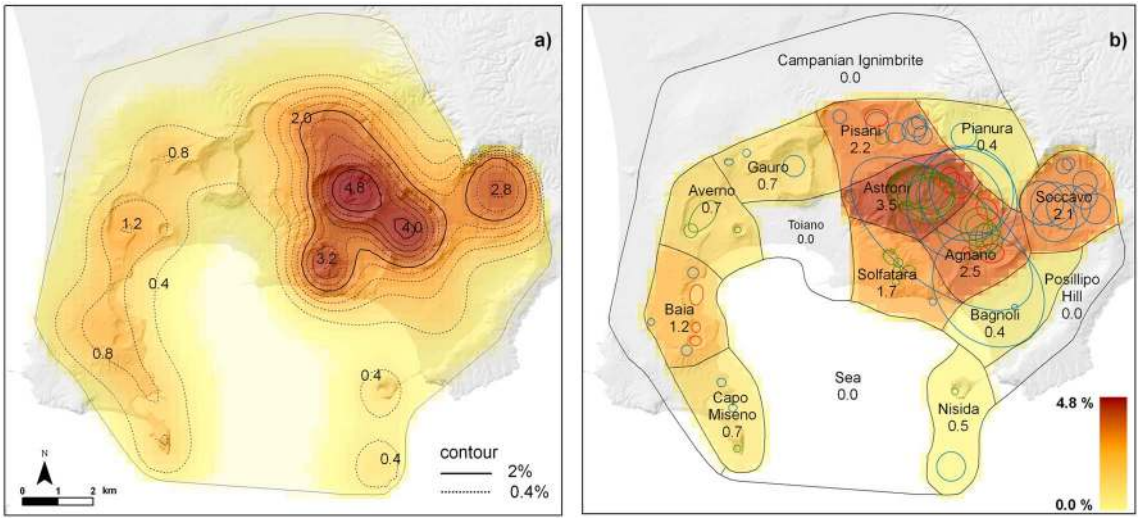

Figure 5. (a) Density distribution of the probability of vent opening obtained by using the vent location data of the three epochs of activity reported in Figures 3 and 4 and a kernel density estimation. Contour and color values indicate the percentage probability of vent opening per km^2 (conditional on the occurrence of an eruption). (b) Density distribution of the probability of vent opening obtained by using the vent location data of the three epochs of activity reported in Figures 3 and 4 and the partitioning of the caldera in 16 homogeneous zones. Values reported in the different subareas indicate the percentage probability of vent opening per km^2 (conditional on the occurrence of an eruption).

concentrated in the central eastern part of the caldera (i.e., Agnano-Astroni-Solfatara; Figures 3 and 4) [*Rosi et al*., 1983; *Di Vito et al*., 1999; *Orsi et al*., 2004; *Isaia et al*., 2009; *Smith et al*., 2011].

The three data sets of vent locations with respect to the three epochs of activity of the volcano (Figures 3 and 4) were the starting point for producing a first spatial distribution of probability of new vent opening, conditional on this information. We adopted two different approaches: a kernel density estimation with Gaussian distributions (Figure 5a) and a simpler probability distribution based on a partition of the caldera into finite zones (Figure 5b). It will be seen that the two approaches are complementary and produce quite consistent results. Both Figures 5a and 5b refer to the whole data set of all vent locations from the three epochs, without discriminating between them. By contrast, in the generation of the final vent opening probability maps vents of different epochs are weighted differently, based on the outcomes of the elicitation.

The kernel density estimation is a nonparametric method for estimating the spatial density of future volcanic events based on the locations of past vents [e.g., *Connor et al*., 2012; *Bebbington and Cronin*, 2011; *Mazzarini et al*., 2013a]. Two important parts of the spatial density estimate are the kernel function and its bandwidth or smoothing parameter. The kernel function can be any positive function K that integrates to one. In general, given a finite sample X_i, $i = 1, \ldots, N$, a kernel density estimator can be defined as

$$f_h(x) = \frac{1}{N}\sum_{i=1}^{N} K\left(\frac{x - X_i}{h}\right)$$

where h is the bandwidth. K is assumed equal to a two-dimensional radially symmetric Gaussian kernel, as with many kernel estimators used in geologic hazard assessments [e.g., *Connor and Hill*, 1995; *Cappello et al*., 2012; *Mazzarini et al*., 2013a]. The bandwidth is typically selected using different theoretical and empirical methods developed for optimizing consistency with data [e.g., *Duong*, 2007; *Mazzarini et al*., 2013a]. Here we took it independent of the spatial location and equal to the mean minimum distance between the centers of the circles/ellipses for each separate epoch since the bandwidth is, in principle and other things being equal, related to the spatial spread of the observed past vents. A complication in our study is that the sample of past vent locations does not comprise points, but areas of uncertainty, and each vent area covers several cells of our grid, some of them completely, others only partially. Therefore, for each cell we took into account the fraction of each vent area that it contains, and then we applied the kernel convolution to this value. In addition, we also assumed that this kernel convolution does not spread the probability outside the CI caldera boundary. An advantage of this approach is that the spatial density estimate will be consistent with the spatial distribution of past volcanic events. A disadvantage of a symmetrical kernel function is that it does not

explicitly allow for geological and structural boundaries and other directional volcanological information [see *Connor et al*., 2012]. The areas with the highest density of past vents are those of Astroni and Agnano (maximum probability per km^2, respectively, around 4.8% and 4.0%) followed by Soccavo, Solfatara, and Pisani (Figure 5a).

The caldera partition approach was developed to take into account this last challenge and to complement the kernel-based approach described above. We subdivided the whole CF caldera into 16 zones, each characterized by internally consistent geological and volcanological features and therefore a quasi-homogeneous distribution of vent opening frequencies. The freedom in drawing the boundary of the zones allows an improved representation of the different geological and morphological features, including those offshore, that characterize each zone as well as the shape of the CI and NYT calderas that define the edge of the CF area and the spatial and temporal clustering of past vents. Apart from the areas between the CI and NYT calderas and the area offshore, where no past vents were located, the different zones had almost equivalent areal sizes so to avoid bias in the analysis. The spatial vent density for each zone was obtained by counting the number (or the fraction) of circles/ellipses of vent locations contained in the zone (Figure 5b). This alternative density distribution is consistent with the density contours obtained by kernel estimation and represents an a posteriori confirmation of the choice of the kernel bandwidth adopted. However, as expected, the computed peak values in the zones are now lower than those obtained with the kernel approach, because within each zone the spatial density is assumed uniform.

The information on vent distribution was integrated with an estimate of the number of lost vents in the three epochs. In several regions within the caldera and also outside it, have been recognized several depositional units that cannot be correlated with identified vents [e.g., *Smith et al*., 2011]. Most of these deposits belong to events that occurred in Epoch I, which is why they are mostly buried below more recent sequences. The lost vents were assumed to be uniformly distributed over the inland portion of the NYT caldera since no vent has been found outside this area, but alternative hypotheses about the location of these vents were also entertained, and their effects on final results investigated.

3.2. Distribution of Faults and Fractures

Faults and fractures represent the other two variables we used as input to the probability map of vent opening potential. Faults and fractures zones are in fact often correlated with the opening of new vents and typically represent a weakness element that may favor magma ascent and eruption. [*Connor et al*., 2000; *Calais et al*., 2008; *Mazzarini et al*., 2013b]. However, the relationships between cropping out faults and fractures and localization of vent openings at CF and other volcanic settings is a complex issue still matter of debate. Several studies of rift zones show a close relationship between extensional regime on the Earth surface and ascending magma. Fields observations, geodetic and geophysical surveys, mathematical models and analog experiments [e.g., *Pollard et al*., 1983; *Mastin and Pollard*, 1988; *Rubin and Pollard*, 1988; *Lister and Kerr*, 1991] indicate that magma generally arises along vertical or steeply dipping dikes which produce subsidence on the Earth surface accommodated by normal faults and fractures. Moreover, the upward magma migration depends on several other features such as the dike-driving overpressure, density and viscosity of magma, and the physical properties of the hosting rocks. Usually, most of the models assume an isotropic and homogeneous upper crust, whereas anisotropic and inhomogeneous features, such as stress barriers and preexisting faults, can also control the pathway of the ascending magma. A sharp change in the elastic properties of the crustal subhorizontal layering and the occurrence of weak layers can produce (i) the arrest of the vertical dike propagation [e.g., *Gudmundsson*, 2003] or (ii) the lateral magma migration [e.g., *Martì et al*., 2013]. Similarly, the existence of moderately dipping shallow inherited faults and fractures can deviate the vertical dike propagation [e.g., *Gaffney et al*., 2007; *Le Corvec et al*., 2013], whereas, on the contrary, major deeply rooted subvertical faults can be preferred paths [*Martì et al*., 2013].

In this study we took advantage of a recent investigation carried out by *Vitale and Isaia* [2014], which described and reconstructed the age, distribution and nature of the different type of faults and fractures located in the CF caldera. As far as faults are concerned, for our purposes, we focused on the map showing the maximum displacement of faults located in a given cell. In this way we assigned a weight not only to the presence of faults but also to the degree of displacement associated with them. In fact, according to *Vitale and Isaia* [2014] and *Isaia et al*. [2015], most of mesoscale faults hosted in the CF caldera are almost vertical with displacements ranging from few centimeters to several meters. Many faults are located close to volcanic

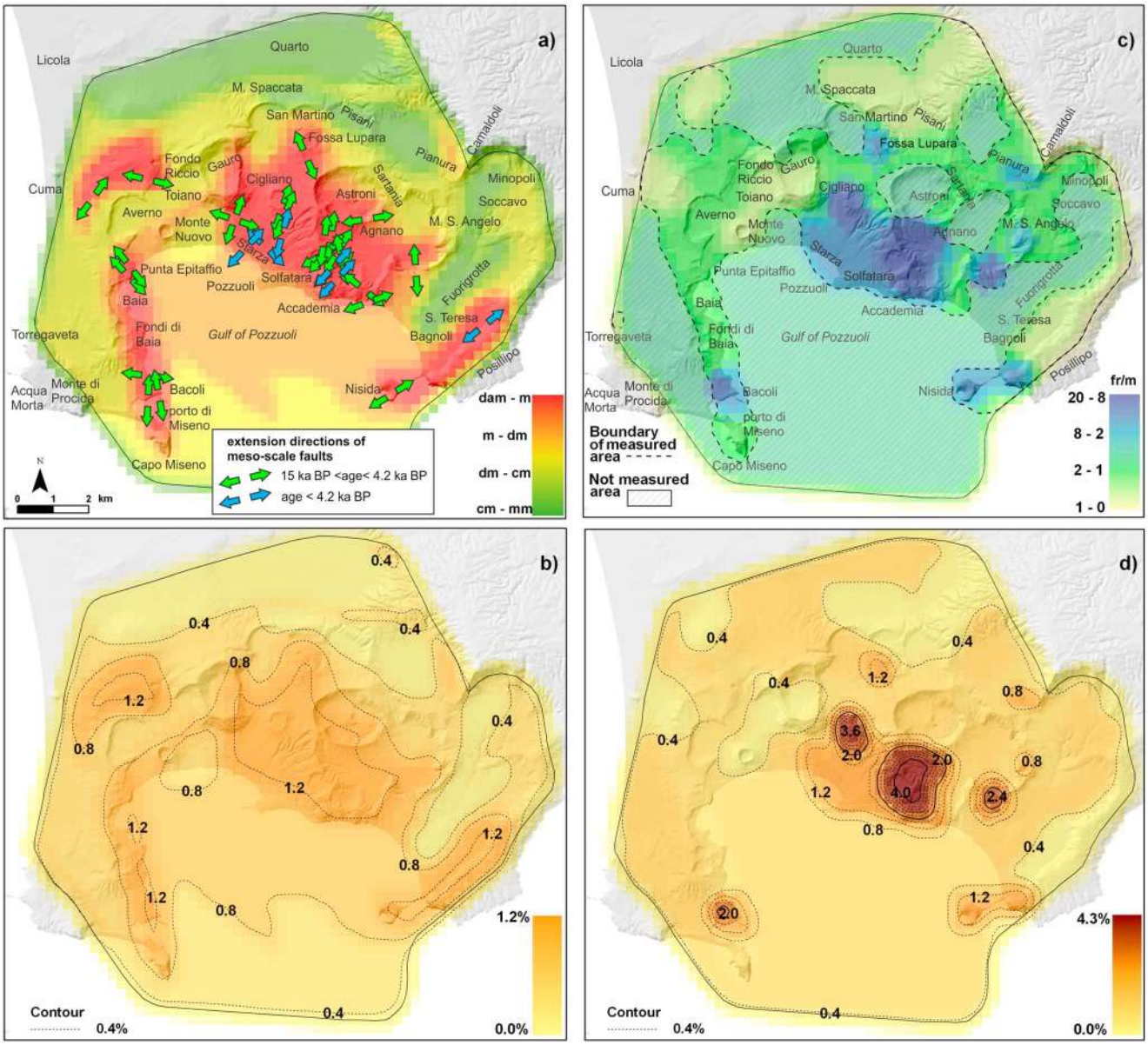

Figure 6. (a) Distribution of the maximum fault displacement in the caldera as derived from the data set of *Vitale and Isaia* [2014]. The four color levels shown correspond to displacements of different orders of magnitude ranging from subcentimetric to metric scales. The figure also shows the extensional directions associated to the main mesoscale faults of the caldera with specific indication of those active in the last 4.2 ka. (b) Density distribution of the probability of vent opening obtained normalizing the values of maximum fault displacement. (c) Distribution of the surface fracture density in the caldera as derived from the data set of *Vitale and Isaia* [2014]. In this case the four colors correspond to different values of density ranging between about 1 and 20 fractures per meter (fr/m). Wide areas of the inland caldera and the offshore part were not measured (dashed areas). In these areas the average value of the total measured zone was assumed. (d) Density distribution of the probability of vent opening obtained normalizing the values of surface fracture density. In Figures 6b and 6d values indicate the percentage probability of vent opening per km^2 (conditional on the occurrence of an eruption).

vents both in the central portion and along the rims of the caldera. The inversion of faults data [*Vitale and Isaia*, 2014] indicates a prevalence of NNE-SSW/NE-SW extensions in the central portion of the caldera, suggesting that an extensional stress field persists since, at least, about 4.2 ka B.P. (Figure 6a).

Given the wide range of displacement observed in the field [*Vitale and Isaia*, 2014], we assigned weights using a (four level) logarithmic (base 10) scale ranging from subcentimetric to metric scales, thus assuming that displacements less than few millimeters are negligible. There were additional assumptions as follows. The value ascribed to each cell was the maximum displacement of the faults cutting the cell. In a case where

no faults were recognized in a given cell due to the presence of overlying geological or anthropic structures, estimates were made using information from regional structures, morphological structures, and lineaments of gravity anomalies [see, e.g., *Florio et al*., 1999; *Capuano et al*., 2013; *Vitale and Isaia*, 2014]. The resulting map (Figure 6a) clearly shows that the larger values of displacement are inferred to be present in the central part of the caldera (e.g., Pozzuoli, Solfatara, and San Vito) and along the eastern and western boarders of the NYT caldera (see also Figure 2). This distribution was then normalized to obtain an integral sum equal to one, and the adjusted distribution used in the definition of the vent opening probability map (see Figure 6b). The resulting map is more homogeneous than the probability maps based solely on the spatial distribution of known past vents, with maximum probability of about 1.2% per km^2 in the areas with greatest displacements, mentioned above.

Fractures were also elements assumed representative of past and present deformation within the caldera and therefore of potentially weakness areas likely exploited by magmatic fluids and indicative of future vent opening [e.g., *Rooney et al*., 2011; *Le Corvec et al*., 2013; *Mazzarini et al*., 2013b]. However, the definition of surface fracture density is particularly challenging due to the sparse, diverse, and incomplete nature of available measurements. These difficulties required a number of simplifying assumptions to be made. The value assigned to each cell was derived by the number of surface fractures measured per meter of survey line length, by naked eye, at each site (see *Vitale and Isaia* [2014] for the locations of the sites). When there was a single measurement site in a cell we simply took that as the measured linear density value, whereas when there were multiple sites we conservatively assumed the highest measured linear density value for caution. Being the fracture density dependent on many factors, including the bed thickness, lithology, and texture [*Bai and Pollard*, 2000; *Guerriero et al*., 2011], the maximum value of density calculated for the lithotype most favorable to fracturing was assumed. In the case where a cell did not contain any measurements, a bilinear interpolation on neighboring cells was assumed.

Nonetheless, the resulting map remained largely incomplete since sizeable areas of the caldera were not close to any measurement. In those parts where measurements were available, weights were assigned proportional to surface fracture density on a linear scale (Figure 6c). Values measured ranged from less than 1 up to about 20 fractures per meter. For areas with no data, a uniform value equal to the average value from the areas with measurements was assigned. The linear scale assumption was based on the fact that fracture openings show small variations, normally <1 mm and rarely larger than a few centimeters [*Vitale and Isaia*, 2014]. By assuming that fracture openings range between 0.2 and 1 mm (where 0.2 mm is the lowest opening threshold for naked eye measurements) [e.g., *Ortega et al*., 2006; *Guerriero et al*., 2011], that fracture density ranges between 1 and 20 fractures per meter, and that they are subvertical, the horizontal displacement ranges from 0.2 to 20 mm per meter.

The highest values of surface fracture density are located in the Solfatara area and around the town of Pozzuoli in the center of the caldera (Figure 6c). These areas correspond also to some regions of intense degassing and hydrothermal activity [*Chiodini et al*., 2012]. Other highly fractured areas are located at Averno, Bacoli-Capo Miseno, Nisida, Posillipo, and part of the Agnano plain. As done for faults, the spatial distribution of fracture density was normalized to sum one across the whole caldera for use it as a component of the vent opening probability map (see Figure 6d): in this way the probability density is defined as directly proportional to the fracture density. Based on this assumption, the maximum percentage probability of vent opening per km^2 reaches values of about 4.3% in the very highly fractured zones, mentioned above, with peak values comparable to the maxima of spatial vent density computed from past events (see Figure 5).

4. Results

Once the five spatial density maps described above were constructed, i.e., the three distributions of vent location in the three epochs, the distribution of maximum fault dislocation and the distribution of the surface fracture density, we applied the structured expert elicitation techniques described in section 2 and Appendix A. As explained above, the maps related to faults and fractures, assimilated here into vent opening probability maps (see Figures 6b and 6d), are strictly maps of maximum fault dislocation and surface fracture density, respectively, this meaning that their contributions to the probability of vent opening are greater where net dislocations and densities are greater. An alternative uniform distribution over the whole caldera area was

Table 1. Probability Percentages of the **Mean** and 5th and 95th Percentiles of the Weight of the Five Variables Considered Together With the Weights of the Lost Vents and Homogeneous Map[a]

Variable/Percentiles	Vents Epoch I	Vents Epoch II	Vents Epoch III	Lost Vents	Faults	Fractures	Homogeneous Map
5%ile	6.3	1.3	10.2	3.3	8.1	5.4	6.3
	9.5	2.2	14.7	4.2	10.2	7.0	8.7
	6.3	1.5	7.6	3.4	5.3	4.3	6.5
Mean	**16.0**	**4.5**	**20.4**	**5.9**	**16.4**	**11.9**	**24.9**
	16.4	**4.8**	**22.5**	**6.3**	**16.5**	**12.3**	**21.3**
	17.7	**4.6**	**19.3**	**6.7**	**13.8**	**12.0**	**25.9**
95%ile	26.7	8.7	33.3	9.0	26.6	20.4	42.4
	24.0	7.6	31.6	8.8	23.9	18.6	31.1
	30.5	9.3	33.8	11.0	24.3	22.0	45.4

[a]The three values reported for the Mean and the 5th and 95th percentiles of each variable (column) refer to, from top to bottom, the CM, ERF, and EW models. The median values (i.e., the 50th percentile) are very similar to the mean values, within about 1%.

also adopted to represent the possibility there may be no correlation between the vent opening distribution and the five variables considered here.

Several elicitation sessions, involving about 10 experts with different volcanological backgrounds (all authors of this paper), were carried out during the 3 year long study through meetings and remote consultations. The main goal was to achieve transparent, robust, and shared estimates of the unknown values of target variables. We carried out the expert calibration by using seed (or test) questions on a mix of CF and Vesuvius volcanism and, more generally, on explosive volcanism [e.g., *Neri et al*., 2008; *Flandoli et al*., 2011].

The elicitation was based upon target questions that followed a hierarchical logic tree structure with various levels (Appendix A; Figure A1 and Table S1 in the supporting information). First, the relevance of the five considered spatial variables was compared to that of the homogeneous distribution. At the next level, the contribution of past vent distributions was compared to those of structural features (i.e., fault displacement and surface fracture density). Moving to the next level, the relative importance of single vents in the three epochs was evaluated as well as the relative weight of the faults and fracture distributions. Additional target questions were related to the number of lost vents in each epoch, based on the stratigraphic evidence available.

4.1. The Weights of the Variables

Table 1 and Figure 7 illustrate, respectively, the percentiles and the density distributions of the weight of the five variables, derived from the elicitation procedure. The weights for lost vents and for the homogeneous map are also included. The weight for lost vents comes from the sum of the products of the number of lost vents in each epoch with the relative weight of a single vent (see Table S1 of the supporting information). Elicitation outcomes are reported for the three different models, i.e., (a) the Classical Model (CM) of *Cooke* [1991], (b) the Expected Relative Frequency (ERF) model of *Flandoli et al*. [2011], and (c) the Equal Weight (EW) model. It appears from the results that the outcomes from the three models are consistent with one another, overall, and do not show any gross differences. As expected the EW model produced wider uncertainties relative to the performance-based CM and the ERF model solutions. In the following we refer mostly to the CM model solutions since it is the most appropriate approach for capturing the uncertainty on unknown values of variables. Quite similar and slightly narrower distributions are computed by the ERF model which, typically, is more precise than the CM in estimating the central value of a distribution. Basic robustness tests show that the CM results are stable when the responses of different subgroups of experts, determined in terms of specific expertise and background, are processed separately; this creates confidence that the elicitation process has reliably and validly synthesized the group's views on the scientific issues involved.

From Table 1 it emerges that the weight assigned to the distribution of the vents of Epoch III is the largest with a value of about 20% (i.e., mean value) and a credible interval between about 10% and 33% (corresponding to the 5th and 95th percentiles, respectively). Weights of about 4.5% and 16% were estimated for the mean of vent distributions of Epoch I and Epoch II, respectively, reflecting to some extent the much larger numbers of vents that occurred in Epoch I. The mean weight of lost vents was estimated at about 6%, with a credible interval between about 3% and 9%. In fact, it was estimated that between 5 and 10 vents were lost from the

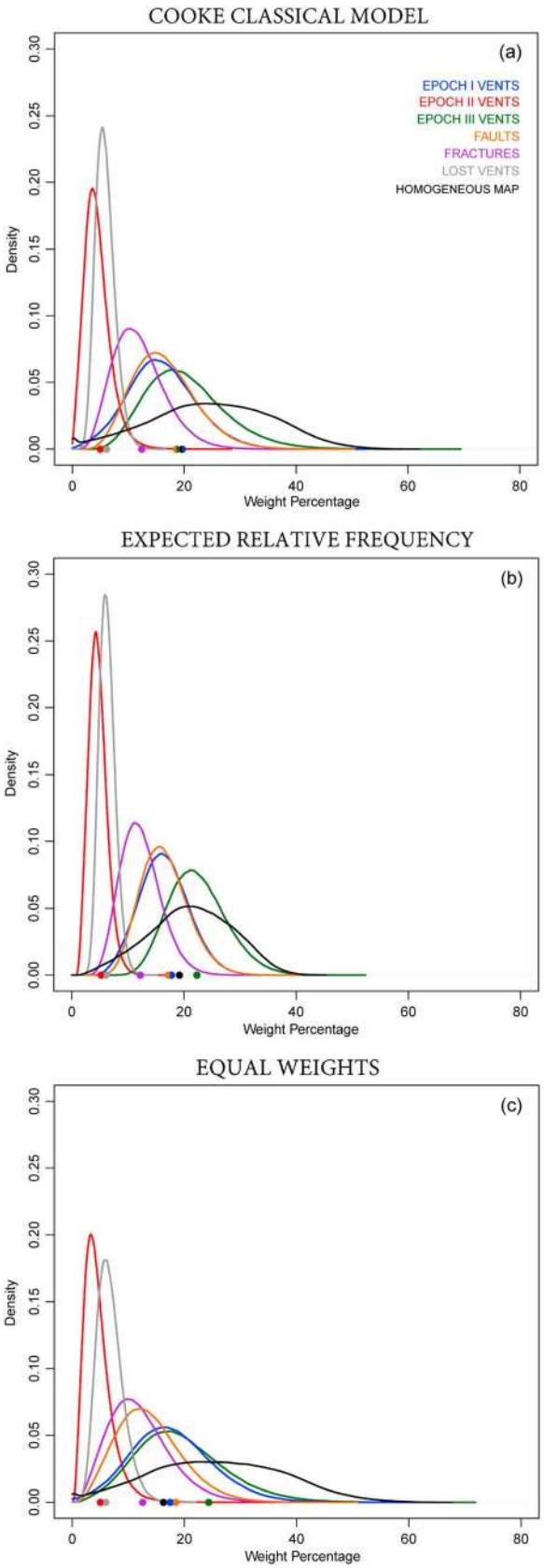

first epoch set, between 0 and 2 from the second epoch and between 1 and 4 from the third epoch (see Table S1 in the supporting information for details). The distribution of fault displacement was weighted about 16.5%, whereas that of fractures about 12% (mean values). Weights of faults and fractures were also affected by significant uncertainty with credible intervals ranging between about 8% and 27% for faults and between about 5% and 20% for fractures. Finally, a mean weight of about 25% was assigned to the homogeneous whole caldera spatial distribution, with credible interval between about 6 and 42%.

Figure 7 represents the densities of the uncertainty spreads for the single weights as well as the central value weights obtained directly from the elicitation, represented as colored dots along the *x* axis. Any discrepancies between these points and the mean values (reported in Table 1) depend on the skewness of the uncertainty distributions. These distributions show again that the CM provides marginally narrower probability density functions with respect to those from EW and that ERF model distributions are still more narrow.

4.2. The Maps of Vent Opening Probability

Finally, Figure 8 shows the vent opening probability maps obtained from weighting and combining the six spatial distributions that were considered. The maps have been computed on the same 100×100 grid with cells of side 250 m used for the distribution of the five variables. The probability of vent opening is expressed as percentage of having a vent per km^2 conditional on the occurrence of a new eruption over the CF caldera (so that the spatial integration of such probability map closes to 100%). The figure reports both the maps obtained using the kernel functions for the density distribution of past vents (Figures 8a–8c) and

Figure 7. Density distribution of the weights of the six variables considered and of the lost vents as a function of the elicitation models assumed, i.e., (a) Cooke CM, (b) ERF model, and (c) EW model. Along the *x* axis are also reported as colored dots the estimates obtained by using just the best guess (central) values provided by the experts.

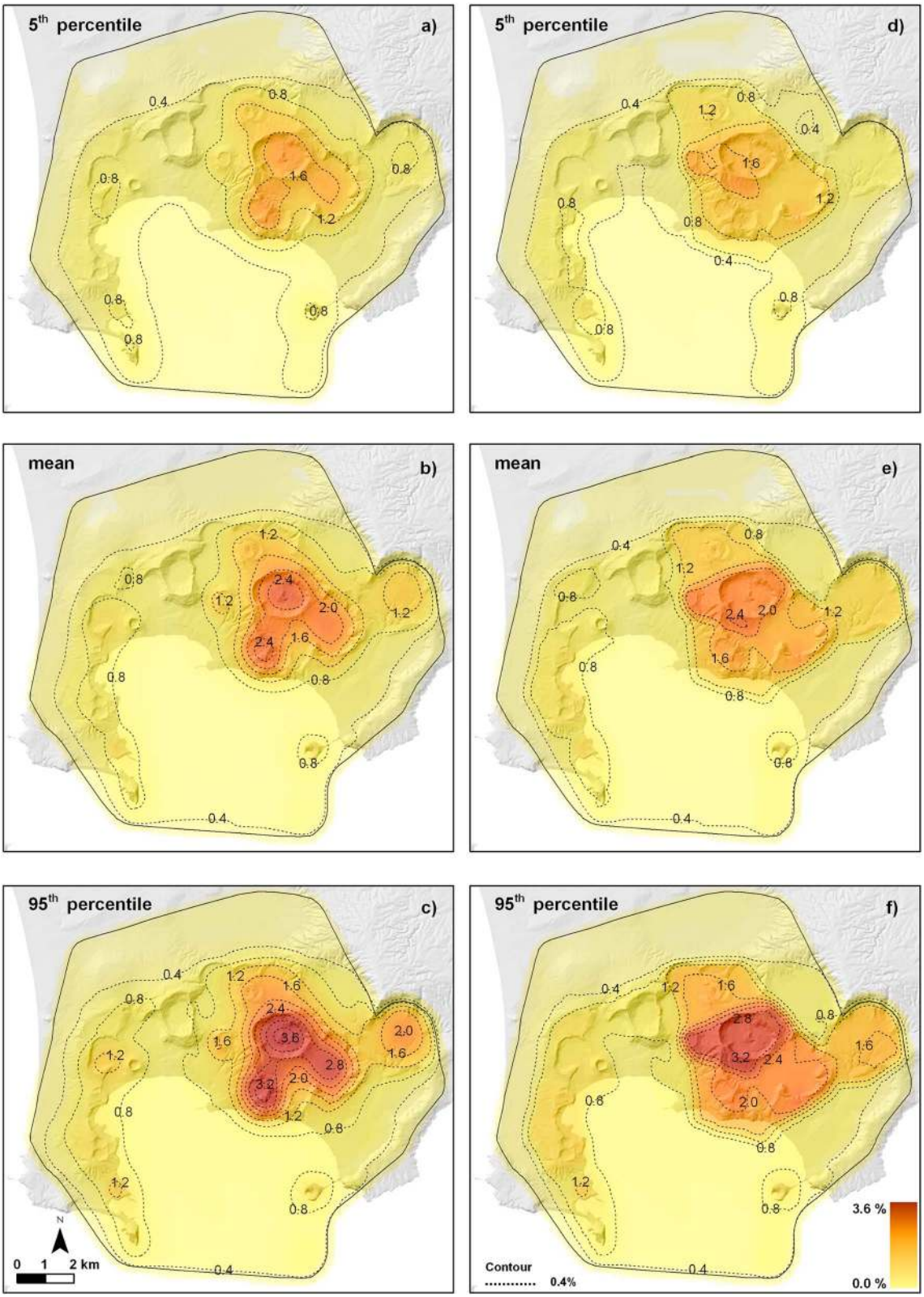

Figure 8. Probability maps of new vent opening as obtained weighting the six variable distributions considered. Contours and colors indicate the percentage probability of vent opening per km^2 (conditional on the occurrence of an eruption). (a–c) The use of kernel functions for the estimate of the density of past vents. (d–f) The partition of the caldera in the 16 homogeneous zones (see text for further explanations). Figures 8a and 8d refer to the 5th percentile, Figures 8b and 8e to the mean values, and Figures 8c and 8f to the 95th percentile. The median maps result very similar to the corresponding mean maps.

the maps obtained using the partitioning of the caldera into sixteen homogeneous zones (Figures 8d–8f). Most importantly, by applying a doubly stochastic model, the vent opening probability maps take into account the sources of epistemic uncertainty quantified here. This means that spatial vent opening probability is not depicted on a single map but through a set of maps which, in the figure, present mean values and 5th and 95th percentiles of the distributions associated with the density values of each cell (corresponding to Figures 8b and 8e, 8a and 8d, and 8c and 8f, respectively). In particular, the spread between such percentiles represents the uncertain correlation of the relevant variables with the position of opening of a new vent and the uncertain number of past vents not included in the eruptive record; however, all of the maps include uncertainties on the locations of past vents. The maps presented here refer to the estimates obtained using the CM solutions and assume that the contribution of lost vents is uniformly distributed over the inland portion of the NYT caldera. Similar maps, not reported here, have been produced by using the other weighting models and assuming different distributions for the lost vents (e.g., similar to those of the identified vents); however, they do not produce significantly different outcomes.

All the maps of Figure 8 show that the vent opening position probability is widely spread over the caldera. With specific reference to the mean probability maps (Figures 8b and 8e), it appears that the probability of vent opening per km^2 is, roughly speaking, greater than 0.4% over all the NYT caldera, with values below about 0.1% just in the area between the NYT and CI calderas, whereas the probability is about 0.2% in the portion of Collina di Posillipo examined. These latter values, in particular, derive from the contribution of the fault and fracture structures existing between the two calderas and on Collina di Posillipo (see Figure 6). No significant differences appear between the probability values on the map based on the kernel functions and those of the map based on caldera partitioning. The probability values of the maps shown in Figures 8d–8f are reported in the Data Sets S1, S2, and S3, respectively, included in the supporting information.

From all the maps, the existence of a wide region of high probability of vent opening, located approximately in the area of Astroni-Agnano-Solfatara, also emerges. Probability values of vent per km^2 up to about 2.4% are predicted by the mean map, from both kernel-based and partition-based maps (Figures 8b and 8e). Credible intervals for these highest values range between about 1.6% and 3.2% (see Figures 8a and 8d and 8c and 8e). The zone of Pisani, north of Astroni, is also characterized by significant values of about 1.2%. In this high-probability region, too, the estimates obtained using the kernel functions are consistent with those obtained using the partitioning. As mentioned above, the main difference is that the kernel distributions concentrate the probability more in the centers of the clusters of past vents, whereas the partition approach distributes the probability uniformly over the single zones, based on broader volcanological and structural features. However, in both cases the highest probabilities were found in the Astroni area.

Outside this higher probability central area, probability of vent opening is quite dispersed with secondary maxima in the zone of Soccavo, in the eastern part of the caldera, and in the zones of Averno-Monte Nuovo-Baia-Capo Miseno, in the western part. At Soccavo, vent opening probability values are about 1.2%; in the western part of the caldera they reach 1% (as mean values). The zones of Gauro-Toiano in the central western part of the caldera appear to be associated with the lowest probability of vent opening; the offshore area is characterized by mean values of about 0.5%.

In Table S2 in the supporting information, we report the estimates of vent opening probability distribution integrated over each of the sixteen zones of the caldera computed using the caldera partitioning and the kernel functions and by adopting the CM, ERF, and EW models.

5. Discussion

The forecast of the location of a future vent is a challenging goal of volcanology and an important element for volcanic hazard assessment. This is particularly true for calderas that typically show eruption behavior patterns significantly more complex than central volcanoes. Most of the known calderas have produced eruption sequences which originated from significantly dispersed vents, difficult to associate into any regular spatiotemporal pattern. Moreover, in most cases explosive eruptions are prevalent and show remarkably variable scales of intensity and magnitude. The way a caldera evolves also favors the development of significantly complex structures, abundant hydrothermal circulation, and thermal anomalies, all of which further complicate the problem and make forecasts particularly uncertain [e.g., *Acocella*, 2007].

CF presents many of the above mentioned properties of calderas. The main characteristics of the CF system are: the presence of a large caldera, produced by two very large explosive eruptions (CI and NYT), with many smaller calderas and craters located inside it; repeated long periods of quiescence, lasting millennia, interrupted by periods of activity lasting several centuries (eruptive epochs); the prevalence of explosive eruptions, and the remarkable spatial scatter of vents active in the last 15 ka over the whole NYT caldera. This latter feature is particularly relevant for CF due to the significant size of the caldera (about 12 km diameter) and the dense urbanization of the territory. A vent opening map is therefore key to providing adequate hazard maps for the main explosive phenomena for which this volcano system is notable.

We have produced several vent opening probability maps based on the latest knowledge of the volcano history and quantifying some of the main epistemic uncertainties identified with this complex volcanic system. In addition to the consideration of the distribution of vents that occurred in the last 15 ka, including the contribution of lost vents, the analysis accounts for the potential influence of faults and surface fractures on the opening of future vents. We assume the presence of these features indicative of areas of upper crustal weakness in the caldera that could affect magma intrusion in a case of unrest. The structural survey of the CF caldera [*Vitale and Isaia*, 2014] indicates that faults and fractures acted in various periods of the last 15 ka of caldera evolution, especially in the central area and along the caldera rims. In particular in the central area the youngest faults (dated from about 4.2 ka to the present, see Figure 6a) show a common extensional stress field characterized by a NNE-SSW/N-S extension that has been interpreted as a favorable condition for possible future magma intrusions. Consideration was also given to the fact that caldera systems are particularly complex and vent opening could be also affected by other variables not accounted for in this analysis. Thus, a uniformly distributed contribution of other influences was assumed over the whole caldera to represent the incompleteness of our knowledge and understanding of the system.

Through several meetings and open discussions, the study participants deliberated in depth on the volcanological data sets to be adopted, as well as their meaning for the specific purpose of this probabilistic analysis. Spreads of opinions were then evaluated and aggregated through structured expert elicitation (see Appendix A), to represent and optimize group judgments. The findings of the analysis were revised through several iterations to fully refine and clarify the data considered and reach an acceptable consensus on outcomes. Findings were also evaluated by adopting alternative elicitation pooling models. The outcomes were found substantially robust with respect to the choice of the expert aggregation method (CM, ERF, or EW), the statistical central value presented (median, mean, or mode of elicited values), and the approach used to produce the probability map based on past vent locations (kernel-based or caldera partitioning).

Based on the expert elicitation outcomes, location distributions of previous vents are judged the most important variables for quantifying the vent opening probability map, with a total contribution weight of about 47% (mean value). This estimate includes a weight of about 6% related to the lost vents. In detail, the location distribution of the vents of Epoch III receives the largest weight (about 20% as mean value) followed by the distribution of the vents of Epoch I and Epoch II with about 16% and 4.5% (as mean values), respectively. During the elicitation, experts were asked to assign weights to the individual vents of each epoch. Then the weight of the vent location distribution for each epoch was computed as the product of the weight of a single vent and the number of vents that occurred in that epoch. This is the reason for the larger relative weight of the location distribution of vents of Epoch I (33 vents) with respect to that of Epoch II (eight vents). The weights ascribed to a single vent in the three epochs at 32%, 33%, and 35% for Epoch I, II, and III, respectively (see Table S1 in the supporting information), were remarkably similar and suggest the experts did not have any meaningful preference for data from one epoch over any other. The distribution of the maximum fault displacement and surface fracture density were weighted (as mean values) about 16% and 12%, respectively. This outcome is related to the fact that for most of the group members, faults appeared more related than fractures to the deep system of the volcano and therefore to the possibility to reflect potential regions of future vent opening. In fact, faults produce much larger deformations than fractures suggesting a closer link to deep processes. Conversely, fractures were considered more representative of the status of the shallow layers of the caldera. Last of all, about 25% weight was assigned to the uniformly homogeneous spatial opening map, i.e., to the possibility that the next vent could open anywhere inside the NYT caldera. Additionally, it is very important to note that from the elicitation, all these weight estimates were characterized by significant associated uncertainties.

Table 2. Extension of the Principal Areal Vent Opening Probability Contours (see Figures 8d–8f): Areas (in km^2) and Percentages of the Whole CF Area, With Associated Uncertainties[a]

Contour	Area (km^2) (5th; Mean; 95th Percentiles)	Percentage of CF Area (5th; Mean; 95th percentiles)
Whole CF	144	100%
0.5% probability	65; **81**; 107	45%; **56%**; 74%
1% probability	23; **31**; 36	16%; **21%**; 25%
2% probability	0.2; **5**; 12	0.1%; **3%**; 8%

[a]The Mean value is reported in bold.

Our final maps (Figure 8), obtained by weighting and combining the five distributions described above plus the lost vents represented as a uniform distribution, provide a quantitative assessment of the spatial probability of vent opening within the caldera. The results highlight the existence of a main, quite wide, region in the central eastern part of the caldera characterized by the highest probabilities of vent opening. This region corresponds to the area of Averno-Agnano-Solfatara. Although the detailed probability distribution in this area depends to some extent on the type of numerical approach used (e.g., kernel functions versus caldera partitioning), the maximum values of vent opening probability per km^2 are in the credible interval [1.6%, 3.2%] with a mean value of about 2.4% in both cases. By spatial integration, the total probability of the next vent opening in this area is about 30% (see also Table S2 in the supporting information). Secondary maxima are obtained in the western part of the caldera, i.e., zones of Averno-Monte Nuovo-Baia-Capo Miseno and in the Soccavo and Pisani areas. These areas are characterized by mean values of about 1–1.2%, i.e., less than half the values estimated for the highest probability area. However, the probability of vent opening is not confined to these areas and, with mean values everywhere above 0.4%, the possibility is widespread over the caldera, thus making the associated background hazard potential broadly distributed in space. It is worth noting also that the last eruption of CF (Monte Nuovo) has occurred in one of the secondary maxima of the computed vent opening probability map and not in the area with the highest probability.

Table 2 reports the total areas of the main vent opening probability contours, the proportions of the whole CF caldera they occupy, expressed as percentages, and the associated uncertainties on these spatial parameters. More than half the caldera has an average probability of vent opening greater than 0.5% and more than one fifth has a probability larger than 1% per km^2. Furthermore, the quantified area uncertainty estimates we provide on these contoured areas should prove valuable when considering confidence levels in mitigation decisions.

It is worth highlighting also that the vent opening probability values per km^2 are associated to a substantial uncertainty range, here represented as (5th percentile − mean)/mean and (95th percentile − mean)/mean; based on inspection of data, it is on average about ±30% of the mean value, with variations from ±10% to ±50% (corresponding to 5th and 95th percentiles) in different areas of the caldera. In particular, uncertainty values spatially change as a function of the variables considered and the way their uncertainties vary and influence the aggregated weights. Estimates of the uncertainty range of integrated probabilities of vent opening on the zones of the caldera partition are also reported in Table S2 in the supporting information.

From inspection of numerical outcomes, the probability of vent opening in the offshore portion of the caldera is about 25 ± 5%. This is a significant value suggesting further investigation of such a possibility would be worthwhile. Also, our knowledge and hence inferences about this portion of the caldera are affected by the lack of information compared to the inland areas (see section 3.2 and Figure 6 about faults and fracture distributions). From the maps created it is also possible to estimate that the mean probability of vent opening in the eastern part of the caldera (assuming the division line between the western and eastern parts coincides with the N-S border dividing the zones of Gauro-Toiano, on the west, from the zones of Pisani-Astroni-Solfatara, on the east) is significantly larger than that in the western part (66% versus 34%, with an uncertainty around ±4%).

Our present results appear qualitatively consistent with those of *Alberico et al.* [2002] and *Orsi et al.* [2004], which suggested the areas in the central eastern part of the caldera are those with the greatest likelihoods of vent opening. They are also semi-quantitatively consistent with those of *Selva et al.* [2012] although, relative to Selva et al., our study indicates the area with the highest likelihood of vent opening (i.e., Astroni-Agnano-Solfatara) has substantially greater probability values than in other parts of the caldera. With reference to mean probability values, the area of Astroni-Agnano-Solfatara has a maximum of 2.4% per km^2, against the 1.9%

reported by Selva et al. Conversely, in the western portion of the caldera the high mean values are about 1% as against 1.5% of Selva et al. In other words, in this study the probability of vent opening appears substantially more concentrated in the central eastern part of the caldera with respect to the estimates of *Selva et al*. [2012], which indicate a main secondary maximum in the western part of the caldera.

Further, *Selva et al*. [2012] report uncertainty ranges of the vent opening probability per km^2 that appear significantly greater than those reported in this study, over the whole caldera: their average spread values correspond to about +180%/−90% of the local mean values, compared with our estimate of ±30%. This is probably due, in part at least, to their assumption of Dirichlet distributions defined with single global dispersion parameters. In contrast, the procedure adopted in our study allows uncertainties to be spatially modulated as a function of the different variables considered.

6. Conclusions

A new spatial map of background probability of future vent opening, conditional on the occurrence of a new eruption in the CF caldera, has been produced by incorporating the most up-to-date information on the distributions of past vents in the last 15 ka, as well as on fault displacement and surface fracture density. The map explicitly accounts, through the application of a doubly stochastic model, for the presence of some relevant sources of epistemic uncertainty in relation to imperfect knowledge of past vent locations, the existence of lost vents, and the relative relevance (i.e., weight) inferred for the different variables considered in the definition of the likelihoods of vent opening. In addition to the mean vent opening map representative of the aleatoric variability of the process, the study produces a set of maps, presented here as upper and lower uncertainty bounds (typically 5th and 95th percentiles) of the vent opening probability at each location. These probability distribution maps were found to be substantially robust with respect to different density estimation methods and expert aggregation models. Given the approach we have followed, our present results could be modified by eliciting the views of a group of experts composed of those who may hold different views from those who participated in this study, but we would be surprised if their findings diverged greatly from ours when the common basis is the same data, knowledge, and process understanding. Of course, our own judgments could be modulated by any substantial new data set, information or interpretation of the CF history and dynamics that might become available in the future.

Our results show evidence for a principal high-probability region in the central eastern portion of the caldera characterized by mean probability values of vent opening per km^2 that are about 6 times greater than the baseline value for the caldera. Significantly lower secondary maxima are found to exist in both the eastern and western parts of the caldera, with probabilities up to about 2–3 times larger than baseline. Nevertheless, the underlying spatial distribution of vent opening position probability is widely dispersed over the whole NYT caldera, including the offshore portion. Most importantly, we accompany our probabilities with quantified epistemic uncertainty estimates which are indicative, typically, of relative spreads ±30% of the local mean value, but with variations between approximately ±10% and ±50%, depending on the location.

Notwithstanding the several assumptions and limitations of the analysis described above, our maps represent crucial input information for the development of quantitative hazard and risk maps of eruptive phenomena in the CF. These maps can be the basis for the generation of up-dated short-term vent opening probability maps, once monitoring information in an impending eruption becomes available. The maps also account for some of the main causes of epistemic uncertainty about the caldera system, although additional sources may still need to be considered. For instance, the method developed here can be further extended to the consideration and incorporation of additional data sets about the volcanological system (together with their uncertainties). Further developments could also consider the temporal and volcanological evolution of the caldera by implementing statistical models able to further explore the time-space structure of this complex system. In the companion paper [*Neri et al.*, 2015], the vent opening probability maps presented here are used to produce first probabilistic background hazard maps for PDC invasion in a future eruption of the CF caldera.

Appendix A: The Expert Elicitation Technique

As discussed in the text, in this study we assumed that the background probability map of new vent opening can be expressed as a linear combination of the five density maps representing the spatial distributions of

past vents (three maps, one for each of the three epochs), maximum fault displacement and surface fracture density, plus an homogeneous map that distributes the probability uniformly over the NYT caldera. The weights are affected by a significant amount of uncertainty representing unknown correlations of these relevant variables with the position of opening of a new vent. To estimate them and their variability, we followed a structured elicitation procedure aimed at acquiring and understanding the experts' opinions about uncertainty quantification for the factors considered. The same technique was used to quantify other relevant unknown variable values, such as the number of lost vents as well as other unknown values for variables used in the mapping of pyroclastic density current hazard [see *Neri et al.*, 2015].

In the following subsections we briefly reprise the key features of the expert elicitation procedure and present the pooling models used, their main outcomes and findings.

A1. Expert Scoring Rules and Weighting Assessments

The concept of expert elicitation concerns the adoption of a formal technique, or techniques, to be used to pool the judgments of a group of experts in order to inform decisions, forecasts, or predictions based on a formalized treatment of uncertainties in relation to the matter under consideration [*Cooke*, 1991; *Aspinall*, 2006]. In this particular study, the objective was not only the elicitation of the unknown value for a variable but also its uncertainty properties. To this aim, we applied three alternative expert scoring/weighting assessment models and we compared the different results obtained.

In general, for a pooling or scoring scheme, the unknown variable values, for which estimates are needed, are called *target items*. During the elicitation procedure, each expert provides three values for every item: their judgment of the central value (represented by the median value of the uncertainty profile) and then interval bounds which express his/her uncertainty about the credible range for the value. In our particular case the 5th and 95th percentiles of the uncertainty distribution were used as marker bounds for the uncertainty distributions. One way to aggregate the answers of a group collectively is that of calculating an equal weights pooling of the experts' densities: such a model is called the *Equal Weights* (EW) solution. This is the first of the three alternative pooling schemes we considered.

However, this way of expressing a group opinion is often not optimal in terms of statistical informativeness: uncertainties tend to be very wide. To estimate value uncertainties accurately and informatively, empirical performance control [*Cooke*, 1991; *Aspinall*, 2006] is needed. With the Classical Model [*Cooke*, 1991], each expert is assigned a weight determined objectively on his/her ability to judge uncertainties with statistical accuracy and informativeness, thus providing a rational basis for pooling the views of a group of experts. In the Classical Model (CM), this empirical control is based on a set of *seed questions*. While actual values of these questions are retrievable, from the literature or other sources, experts are not expected to know them precisely but are expected to be able to define credible ranges that capture the values by informed reasoning. In our case the seed questions were about carefully researched aspects of Campi Flegrei volcanism, other Italian volcanoes, such as Vesuvius, and about explosive volcanism in general. Experts' weights were then computed using the mathematical scoring rule process described in *Cooke* [1991], with the resulting combination of experts' assessments on each *target* item referred to as a "Decision Maker" (DM).

Here we will briefly compare and contrast the Classical Model (CM) with a complementary approach, the Expected Relative Frequency model (ERF) [*Flandoli et al.*, 2011], and note that these methods are based on similar but crucially different scoring rule philosophies.

The CM quantifies an expert's score as the product of two empirically determined measures, *calibration* and *informativeness*. The calibration score rewards good ability in an expert to be statistically accurate when assigning values to probability outcomes against known values. Thus, a "well calibrated" expert provides answers such that the real values are symmetrically balanced with respect to his/her 50th percentile markers, and the majority fall between his/her 5th and 95th percentiles (but not necessarily all). The information score reflects an expert's capacity to provide concentrated distributions over the same variables. On its own, the information score does not consider the expert's distribution locations relative to the true realization values; instead, it is the average relative information over all the seed questions, with respect to a uniform distribution. But the CM takes the product of these two scores to reward jointly an expert with statistical accuracy and informativeness. Furthermore, the CM also performs optimization to maximize the resulting group decision maker score (treating the DM as added "expert").

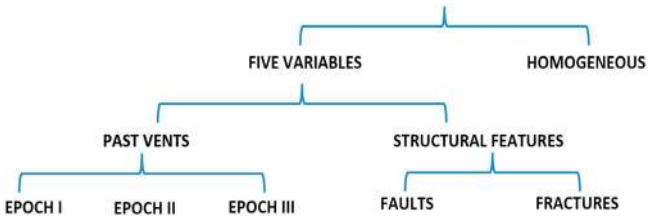

Figure A1. Hierarchical logic tree structure associated to the target questions queried during the elicitation sessions.

The *Expected Relative Frequency model* [*Flandoli et al.*, 2011] computes a score for each seed item (i.e., the same calibration questions used in the CM) by integrating the probability density function over an interval centered around the true value. The idea of this model is that the expert's score is high if his/her mode is close to the true value (in relative error), but the score is modulated by the uncertainty declared by the expert. The average of an expert's scores over all the seed questions can be interpreted as the "expected accuracy" of the expert [*Flandoli et al.*, 2011]. In particular, if for each seed question a random variable is defined with the uncertainty distribution of a chosen expert, then his/her ERF score is the expectation of the fraction of these random variables that fall in a selected interval around the true values.

Relative to Equal Weights, and each other, in general the CM provides better quantification of variable uncertainty for multiple items, whereas the ERF model can provide more reliable estimates for central values. More information on the differences between the three models and their performance can be found in *Flandoli et al.* [2011].

A2. The Logic Tree Questionnaire, Linear Weights, and Elicitation Outcomes

To simplify the quantification of the weight to assign to each spatial distribution for the definition of the vent opening probability map, we defined a simple hierarchical logic tree (see Figure A1). Most of the target questions that were asked quantify the relative importance, or relevance, of one variable or feature of the system versus others. In each of these comparisons, the best estimate (central) percentages should sum close to 100%; strictly, the distribution means should sum to 100%, and the sum of elicited medians may diverge slightly depending upon tail asymmetries; elicited distributions can be normalized if necessary. Experts were asked to evaluate the uncertainties associated with their judgments of relative importance. The first question was about the relative importance of the five different distributions considered taken jointly (see section 3, above) compared to that of the uniform distribution, here assumed to represent the lack of information. At the next hierarchical level, the contribution of the overall past vent distribution was compared to that of the current structural features of the caldera (i.e., fault maximum displacement and surface fracture density). At the next level of the tree, the relative weights of single vents of the three epochs and the relative weights of faults and fracture distributions were evaluated. Other relevant questions were about the estimation of the number of lost vents in each epoch of activity, due to the successive eruptions and the morphological, volcanological, and man-made transformations of the caldera and to other variables with unknown values which might be relevant for the mapping of pyroclastic density current hazard [see *Neri et al.*, 2015]. We report in Table S1 in the supporting information the abbreviated questionnaire protocol and the corresponding CM, ERF, and EW outcomes.

To calculate the weights and their uncertainty characteristics for each of the three elicitation methods adopted, the three percentiles of the CM global DM were used to define triangular distributions, from which randomized values could be sampled for each question. We followed a Monte Carlo simulation approach for determining these single-branch weight estimates, normalizing complementary values to sum to one, and then multiplying the single weights over each branch of the logic tree. In this way we obtained a large sample of randomized weights to assign to the six maps of the relevant spatial distributions, i.e., the distribution of past vents from the three epochs, the distribution of lost vents, assumed uniform, the fault and fracture distributions, and the uniform homogenous map over the NYT caldera (see Table 1 and Figure 7).

Each vector sample of the weights of the distributions (along with a sample of the number of lost vents of each epoch) can therefore be convolved into a probability map of new vent opening, obtained using those weights. To visualize the variability of these maps, we computed "average maps" by Monte Carlo simulation, plotted as mean or median maps, as appropriate, and two maps representing the "uncertainty bounds" of the distribution, expressed as the 5th and 95th percentiles of the values sampled (see Figure 8).

Finally, Table S2 in the supporting information reports the integrated probabilities on the zones of our caldera partition (see section 3.1 of the main text), using the three scoring models CM, ERF, and EW and the two approaches based on caldera partitioning and on the kernel density estimation. The outcomes allow comparison of findings from the elicitation methods and from the density estimation methods. From inspection, it appears that the results overall are sensibly consistent with each other and that average discrepancies of mean values are generally below about 1%. Similarly, the upper and lower percentiles expressing the uncertainty bounds are substantially consistent between the different models. These outcomes confirm again that the CM and the ERF models produce narrower uncertainty distributions than the EW model. It is worth noting also that the distribution mean values and central values (medians obtained directly from the elicitation) are remarkably similar to one another, and some significant differences arise only with the EW solutions.

Acknowledgments

In addition to the tables and data sets included in the supporting information, other data sets and computer codes used to generate the results as well as derived data can be requested to the corresponding author (A.N.). This work has been partially developed during the projects "V1—Stima della pericolosità vulcanica in termini probabilistici" and "Speed—Scenari di pericolosità e danno dei vulcani della Campania", funded by Dipartimento della Protezione Civile (Italy) and Regione Campania (Speed). Partial support was also provided by the EU-funded MEDSUV project (grant 308665) and the COST Action Expert Judgement Network (IS1304). W.P.A. was also partially supported at Bristol University by an ERC Advanced Research Grant to R.S.J. Sparks (VOLDIES) and by the Natural Environment Research Council (Consortium on Risk in the Environment: Diagnostics, Integration, Benchmarking, Learning and Elicitation —CREDIBLE; grant NE/J017450/1). The contribution and support of ideas of many colleagues participating to the above projects are acknowledged. In particular, Céline Fourmentraux significantly contributed to the initial part of this work. The manuscript does not necessarily represent official views and policies of the Dipartimento della Protezione Civile. The authors also acknowledge the thorough reviews of J. Martì and G. Valentine and useful discussions with F. Mazzarini, which significantly improved the paper.

References

Acocella, V. (2007), Understanding caldera structure and development: An overview of analogue models compared to natural calderas, *Earth Sci. Rev.*, *85*, 125–160.

Alberico, I., L. Lirer, P. Petrosino, and R. Scandone (2002), A methodology for the evaluation of long-term volcanic risk from pyroclastic flows in Campi Flegrei (Italy), *J. Volcanol. Geotherm. Res.*, *116*, 63–78.

Aspinall, W. P. (2006), Structured elicitation of expert judgment for probabilistic hazard and risk assessment in volcanic eruptions, in *Statistics in Volcanology*, Geological Society of London on behalf of IAVCEI, edited by H. M. Mader et al., 296 pp., Geological Society for IAVCEI, London.

Bai, T., and D. D. Pollard (2000), Fracture spacing in layered rocks: A new explanation based on the stress transition, *J. Struct. Geol.*, *22*, 43–57.

Bartolini, S., A. Cappello, J. Martì, and C. Del Negro (2013), Q-VAST: A new Quantum GIS plug-in for estimating volcanic susceptibility, *Nat. Hazards Earth Syst. Sci.*, *13*, 3031–3042.

Bebbington, M. S., and S. J. Cronin (2011), Spatio-temporal hazard estimation in the Auckland Volcanic Field, New Zealand, with a new vent-order model, *Bull. Volcanol.*, *73*, 55–72.

Berrino, G., G. Corrado, G. Luongo, and B. Toro (1984), Ground deformation and gravity changes accompanying the 1982 Pozzuoli uplift, *Bull. Volcanol.*, *47*, 187–200.

Bisson, M., A. Fornaciai, and F. Mazzarini (2007), SITOGEO: A geographic database used for GIS applications, *Il Nuovo Cimento C - Note Brevi*, *30C*(3), doi:10.1393/ncc/i2007-10243-9.

Calais, E., et al. (2008), Strain accommodation by slow slip and dyking in a youthful continental rift, East Africa, *Nature*, *456*, 783–788.

Cappello, A., M. Neri, V. Acocella, G. Gallo, A. Vicari, and C. Del Negro (2012), Spatial vent opening probability map of Etna volcano (Sicily, Italy), *Bull. Volcanol.*, *74*, 2084–2094.

Capuano, P., G. Russo, L. Civetta, G. Orsi, M. D'Antonio, and R. Moretti (2013), The active portion of the Campi Flegrei caldera structure imaged by 3-D inversion of gravity data, *Geochem. Geophys. Geosyst.*, *14*, 4681–4697, doi:10.1002/ggge.20276.

Chapman, N., et al. (2012), TOPAZ Project: Long-term tectonic hazard to geological repositories, Nuclear Waste Management Organization of Japan (NUMO) Report, 87 pp.

Chiodini, G., S. Caliro, P. De Martino, R. Avino, and F. Ghepardi (2012), Early signals of new volcanic unrest at Campi Flegrei caldera? Insights from geochemical data and physical simulations, *Geology*, *40*, 943–946.

Connor, C. B., and B. E. Hill (1995), Three nonhomogenous Poisson models for the probability of basaltic volcanism: Application to the Yucca Mountain region, Nevada, *J. Geophys. Res.*, *100*, 10,107–10,125, doi:10.1029/95JB01055.

Connor, C. B., J. A. Stamatakos, D. A. Ferrill, B. E. Hill, G. I. Ofoegbu, F. M. Conwey, B. Sagar, and J. Trapp (2000), Geologic factors controlling patterns of small-volume basaltic volcanism: Application to a volcanic hazards assessment at Yucca Mountain, Nevada, *J. Geophys. Res.*, *105*, 417–432, doi:10.1029/1999JB900353.

Connor, L., C. B. Connor, K. Meliksetian, and I. Savov (2012), Probabilistic approach to modeling lava flow inundation: A lava flow hazard assessment for a nuclear facility in Armenia, *J. Appl. Volcanol.*, *1*, 3, doi:10.1186/2191-5040-1-3.

Cooke, R. M. (1991), *Experts in Uncertainty: Opinion and Subjective Probability in Science*, 336 pp., Oxford Univ. Press, New York.

D'Oriano, C., E. Poggianti, A. Bertagnini, R. Cioni, P. Landi, M. Polacci, and M. Rosi (2005), Changes in eruptive style during the AD 1538 Monte Nuovo eruption (Phlegrean Fields, Italy): The role of syn-eruptive crystallization, *Bull. Volcanol.*, *67*, 601–621.

De Vivo, B., G. Rolandi, P. B. Gans, A. Calvert, W. A. Bohrson, F. J. Spera, and A. E. Belkin (2001), New constraints on the pyroclastic eruption history of the Campanian volcanic plain (Italy), *Mineral. Petrol.*, *73*, 47–65.

Deino, A. L., G. Orsi, S. De Vita, and M. Piochi (2004), The age of the Neapolitan Yellow Tuff caldera-forming eruption (Campi Flegrei caldera, Italy) assessed by 40Ar/39Ar dating method, *J. Volcanol. Geotherm. Res.*, *133*, 157–170.

Del Gaudio, C., I. Aquino, G. P. Ricciardi, C. Ricco, and R. Scandone (2010), Unrest episodes at Campi Flegrei: A reconstruction of vertical ground movements during 1905–2009, *J. Volcanol. Geotherm. Res.*, *195*, 48–56.

Di Vito, M. A., L. Lirer, G. Mastrolorenzo, and G. Rolandi (1987), The Monte Nuovo eruption of Campi Flegrei, Italy, *Bull. Volcanol.*, *49*, 608–615.

Di Vito, M. A., R. Isaia, G. Orsi, J. Southon, S. De Vita, M. D'Antonio, L. Pappalardo, and M. Piochi (1999), Volcanism and deformation since 12000 years at the Campi Flegrei caldera (Italy), *J. Volcanol. Geotherm. Res.*, *91*, 221–246.

Duong, T. (2007), Ks: Kernel density estimations and kernel discriminant analysis for multivariate data in R, *J. Stat. Software*, *21*, 1–16.

Dvorak, J. J., and P. Gasparini (1991), History of earthquakes and vertical ground movement in Campi Flegrei caldera, southern Italy: Comparison of precursory events to the A.D. 1538 eruption of Monte Nuovo and of activity since 1968, *J. Volcanol. Geotherm. Res.*, *48*, 77–92.

Flandoli, F., E. Giorgi, W. P. Aspinall, and A. Neri (2011), Comparison of a new expert elicitation model with the Classical Model, equal weights and single experts, using a cross-validation technique, *Reliab. Eng. Syst. Saf.*, *96*, 1292–1311.

Florio, G., M. Fedi, F. Cella, and A. Rapolla (1999), The Campanian Plain and Phlegrean Fields: Structural setting from potential field data, *J. Volcanol. Geotherm. Res.*, *91*, 361–37.

Gaffney, E. S., B. Damjanac, and G. A. Valentine (2007), Localization of volcanic activity: 2. Effects of pre-existing structure, *Earth Planet. Sci. Lett.*, *263*, 323–338.

Giaccio, B., R. Isaia, F. Fedele, E. Di Canzio, J. Hoffecker, A. Ronchitelli, A. Sinitsyn, M. Anikovich, S. Lisitsyn, and V. Popov (2008), The Campanian Ignimbrite and Codola tephra layers: Two temporal/stratigraphic markers for the Early Upper Palaeolithic in southern Italy and eastern Europe, *J. Volcanol. Geotherm. Res.*, *177*, 208–226.

Gudmundsson, A. (2003), Surface stresses associated with arrested dykes in rift zones, *Bull. Volcanol.*, *65*, 606–619.
Guerriero, V., S. Vitale, S. Ciarcia, and S. Mazzoli (2011), Improved statistical multi-scale analysis of fractured reservoir analogues, *Tectonophysics*, *504*, 14–24.
Guidoboni, E., and C. Ciuccarelli (2011), The Campi Flegrei caldera: Historical revision and new data on seismic crises, bradyseisms, the Monte Nuovo eruption and ensuing earthquakes (twelfth century 1582 AD), *Bull. Volcanol.*, *73*, 655–677.
Isaia, R., P. Marianelli, and R. Sbrana (2009), Caldera unrest prior to intense volcanism in Campi Flegrei (Italy) at 4.0 ka B.P.: Implications for caldera dynamics and future eruptive scenarios, *Geophys. Res. Lett.*, *36*, L21303, doi:10.1029/2009GL040513.
Isaia, R., S. Vitale, M. G. Di Giuseppe, E. Iannuzzi, F. D. A. Tramparulo, and A. Troiano (2015), Stratigraphy, structure and volcano-tectonic evolution of Solfatara maar-diatreme (Campi Flegrei, Italy), *Geol. Soc. Am. Bull.*, doi:10.1130/B31183.1, in press.
Le Corvec, N., T. Menand, and J. Lindsay (2013), Interaction of ascending magma with pre-existing crustal fractures in monogenetic basaltic volcanism: An experimental approach, *J. Geophys. Res. Solid Earth*, *118*, 968–984, doi:10.1002/jgrb.50142.
Lister, J. R., and R. C. Kerr (1991), Fluid-mechanical models of crack propagation and their application to magma transport in dykes, *J. Geophys. Res.*, *96*, 10,049–10,077, doi:10.1029/91JB00600.
Martì, J., and A. Felpeto (2010), Methodology for the computation of volcanic susceptibility: An example for mafic and felsic eruptions on Tenerife (Canary Islands), *J. Volcanol. Geotherm. Res.*, *195*, 69–77.
Martì, J., V. Pinel, C. López, A. Geyer, R. Abella, M. Tárraga, M. J. Blanco, A. Castro, and C. Rodríguez (2013), Causes and mechanisms of El Hierro submarine eruption (2011–2012) (Canary Islands), *J. Geophys. Res. Solid Earth*, *118*, 1–17, doi:10.1002/jgrb.50087.
Mastin, L. G., and D. D. Pollard (1988), Surface deformation and shallow dike intrusion processes at Inyo Craters, Long Valley, California, *J. Geophys. Res.*, *93*, 13,221–13,235, doi:10.1029/JB093iB11p13221.
Mazzarini, F., D. Keir, and I. Isola (2013a), Spatial relationship between earthquakes and volcanic vents in the central-northern Main Ethiopian Rift, *J. Volcanol. Geotherm. Res.*, *262*, 123–133.
Mazzarini, F., T. O. Rooney, and I. Isola (2013b), The intimate relationship between strain and magmatism: A numerical treatment of clustered monogenetic fields in the Main Ethiopian Rift, *Tectonics*, *32*, 49–64, doi:10.1029/2012TC003146.
Neri, A., et al. (2008), Developing an event tree for probabilistic hazard and risk assessment at Vesuvius, *J. Volcanol. Geotherm. Res.*, *178*, 397–415.
Neri, A., et al. (2015), Quantifying volcanic hazard at Campi Flegrei caldera (Italy) with uncertainty assessment: 2. Pyroclastic density current invasion maps, *J. Geophys. Res. Solid Earth*, doi:10.1002/2014JB011776.
Orsi, G., M. D'Antonio, S. De Vita, and G. Gallo (1992), The Neapolitan Yellow Tuff, a large-magnitude trachytic phreatoplinian eruption; eruptive dynamics, magma withdrawal and caldera collapse, *J. Volcanol. Geotherm. Res.*, *53*, 275–287.
Orsi, G., M. A. Di Vito, and R. Isaia (2004), Volcanic hazard assessment at the restless Campi Flegrei caldera, *Bull. Volcanol.*, *66*, 514–530.
Ortega, O., R. Marrett, and E. Laubach (2006), Scale-independent approach to fracture intensity and average spacing measurement, *AAPG Bull.*, *90*, 193–208.
Pollard, D. D., P. T. Delaney, W. A. Duffield, E. T. Endo, and A. T. Okamura (1983), Surface deformation in volcanic rift zones, *Tectonophysics*, *94*, 541–584.
Rittmann, A. (1950), Sintesi Geologica dei Campi Flegrei, *Boll. Soc. Geol. It.*, *LXIX-II*, 117–128.
Rooney, T. O., I. D. Bastow, and D. Keir (2011), Insights into extensional processes during magma assisted rifting: Evidence from aligned scoria cones and maars, *J. Volcanol. Geotherm. Res.*, *201*, 83–96.
Rosi, M., and A. Sbrana (Eds) (1987), *Phlegraean Fields, Quaderni della Ricerca Scientifica*, vol. 114, pp. 175, CNR, Roma.
Rosi, M., A. Sbrana, and C. Principe (1983), The Phlegrean Fields: Structural evolution, volcanic history and eruptive mechanisms, *J. Volcanol. Geotherm. Res.*, *17*, 273–288.
Rubin, A. M., and D. D. Pollard (1988), Dike-induced faulting in rift zones of Iceland and Afar, *Geology*, *16*, 413–417.
Scarpati, C., A. Perrotta, S. Lepore, and A. Calvert (2012), Eruptive history of Neapolitan Volcanoes: Constrains from 40Ar-39Ar dating, *Geol. Mag.*, *150*(3), 412–425.
Selva, J., G. Orsi, M. A. Di Vito, W. Marzocchi, and L. Sandri (2012), Probability hazard map for future vent opening at the Campi Flegrei caldera (Italy), *Bull. Volcanol.*, *74*, 497–510.
Smith, V. C., R. Isaia, and N. J. G. Pearce (2011), Tephrostratigraphy and glass compositions of post-15 ka Campi Flegrei eruptions: Implications for eruption history and chronostratigraphic markers, *Quat. Sci. Rev.*, *30*, 3638–3660.
Vitale, S., and R. Isaia (2014), Fractures and faults in volcanic rocks (Campi Flegrei, Southern Italy): Insights into volcano-tectonic processes, *Int. J. Earth Sci.*, *103*, 801–819, doi:10.1007/s00531-013-0979-0.